Hindawi Publishing Corporation
Advances in Meteorology
Volume 2014, Article ID 206352, 12 pages
http://dx.doi.org/10.1155/2014/206352

Research Article

Aircraft Observations of Ice Particle Properties in Stratiform Precipitating Clouds

Tuanjie Hou,[1] Hengchi Lei,[1,2] Zhaoxia Hu,[1] and Jun Zhou[1]

[1] *Laboratory of Cloud-Precipitation Physics and Severe Storms, Institute of Atmospheric Physics, Chinese Academy of Sciences, Beijing 100029, China*
[2] *Collaborative Innovation Center on Forecast and Evaluation of Meteorological Disasters, Nanjing University of Information Science & Technology, Nanjing 210044, China*

Correspondence should be addressed to Tuanjie Hou; houtuanjie@gmail.com

Received 10 July 2013; Revised 16 February 2014; Accepted 28 February 2014; Published 14 April 2014

Academic Editor: Harry D. Kambezidis

This study presented airborne measurements of ice particle properties in three stratiform precipitating clouds over northern China. By using horizontal observations at selected altitudes, the distributions of ice water content (IWC), particle habits, and particle size spectrum parameters were investigated. The cloud cases were characterized by high IWC values due to the existence of embedded convective cells. Liquid water contents were rather low with the maxima of less than 0.3 g m^{-3} and the general values of less than 0.1 g m^{-3}. The occurrence of large dendritic crystals as well as rimed capped columns and branched crystals indicated that ice seeding from the above cloud layer (6 km altitude or above) contributed significantly to both high ice crystal number concentrations and IWCs. Horizontal observations at selected levels suggested the general decreasing trend of IWC with decreasing temperature only in part of the cloud layers but not throughout the cold layer of the multilayered stratiform clouds. Both exponential and gamma functions were used to characterize the particle size spectrum parameters. The slope parameter values of exponential distributions were primarily in the range of 10^3–10^4 m^{-1}. In comparison, slope values of the gamma distribution fits spanned more and a relationship was found between the dispersion and slope values.

1. Introduction

Ice particles in ice or mixed-phase clouds have been investigated in many previous studies [1–3], and they are complex in concentrations, habits, and relative growth modes, affecting precipitation processes and radiative transfer. Furthermore, the study of ice particle size distributions is critical for developing parameterizations for mesoscale and climate models [4].

The extensive use of airborne cloud probes has made it possible to quantitatively examine particle properties by measuring cloud particle sizes and images. Sekhon and Srivasta [5] concluded that the size distribution of snowflakes can be described using the exponential relation. By measuring the size distribution of precipitation particles in frontal clouds, Houze Jr. et al. [6] also found that particles with sizes larger than 1.5 mm generally follow an exponential size distribution. Since devising the spiral decent flight plan by Lo and Passarelli Jr. [7], it has been improved and used in studies of ice particle spectra evolution [8–10]. Heymsfield et al. [11] and Field et al. [12] presented parameterizations to estimate moments of snow size distributions that can be used in numerical models. Woods et al. [13] subgrouped size distributions of snow particles according to the habit composition from airborne imagery, which significantly improved correlations between the size spectrum parameters and temperature. Aircraft observations of particle size spectra were parameterized in cloud-resolving models in the 1980s in China. Case studies of cloud particle spectra in stratiform clouds over northern China [14, 15] have also been conducted in recent years, but there are still large uncertainties in quantifying cloud microphysical properties [16].

Apart from the above particle information, ice water content (IWC) is also an important parameter to characterize cloud microphysical properties. There are two ways to obtain ice water content from airborne data: one way is *in situ*

measurements based on condensed- and gas-phase water [17] and the other way is by calculation from measured ice particle sizes and images [18–20]. For airborne observations without direct IWC measurement, mass-dimensional relationships for ice particles are very useful to analyze microphysical structure and particle growth modes. Fleishauer et al. [21] investigated IWC profiles within six midlevel clouds by using the mass-dimensional expressions from Mitchell et al. [18]. Brown and Francis [19] introduced an improved method to estimate IWC from the mass-dimensional relationships. Gallagher et al. [22] discussed microphysical variations in tropical anvil cirrus outflow regions with the IWC calculated from Heymsfield et al. [23]. The vertical profiles of IWC in midlatitude mixed-phase clouds have also been studied with such method of IWC estimation [24, 25].

Since mixed-phase stratiform clouds are important in producing precipitation over northern China, numerous aircraft observations have been conducted since the 1980s [16, 26, 27]. However, horizontal traverses at a variety of altitudes within one cloud system did not occur frequently. The objective of this study is to investigate the characteristics of IWC distribution and ice particle size spectrum parameters at selected altitudes by using the aircraft data collected in 2009 and 2010. Ice crystal habits at corresponding altitudes are also compared to provide further insight into particle growth mechanisms.

2. Instrumentation and Data Processing

2.1. Instrumentation. Two Y-12E aircraft, from the Shanxi and Beijing Weather Modification Bureaus, equipped with cloud microphysical probes manufactured by droplet measurement technology (DMT) were used to conduct aircraft observations. The Shanxi aircraft was instrumented with a cloud droplet probe (CDP) with a size range of 2–50 μm, a 2D cloud imaging probe (CIP) with a size range of 25–1550 μm, and a precipitation imaging probe (PIP) with a size range of 100–6200 μm. The CIP has a laser diode array of 64 elements, but particles shadowing an end diode are rejected. Therefore, up to 62 slices compose a particle image. In addition, the individual elements of the diode array must be 70% occulted to trigger the digital electronics for an accepted particle. The Beijing aircraft was equipped with a cloud, aerosol, and precipitation spectrometer (CAPS), including a cloud and aerosol spectrometer (CAS) with a size range of 0.6–50 μm, and with a CIP and PIP with the same size ranges as those in the Shanxi aircraft. In addition to the above probes, the two aircraft were also equipped with cloud condensation nuclei counter (CCN) and LWC-100, but data from those probes were not considered in the study due to poor baselining before observations.

2.2. IWC Calculation. For cloud particle observations using imaging probes, the number of fragments in the images of shattered particles may reach several hundreds, so the shattering effect should be considered during data analysis [28, 29]. Field et al. [30] found that estimated IWC could be overestimated by 20–30% for narrow size distributions due to the shattering process. And they demonstrated that fragmented particles could be filtered by considering interarrival times. A large quantity of particles smaller than 100 μm was found during some flights and concentrations for those small particles were not included in particle size distributions [31]. Due to lack of reliable statistics on shattering effects for aircraft observations in China, only particles larger than 100 μm were considered valid for IWC and particle size parameter calculation in this study. The IWC estimation was based on the combined measurements with particles smaller than 1000 μm measured by the CIP and particles larger than 1000 μm measured by the PIP.

Ice water content can be calculated based on the mass-dimensional relationship of Heymsfield et al. [23] (H04):

$$m(D) = 0.0219D^{2.6}, \quad (1)$$

where m (g) represents the mass of an ice particle and D (cm) is the maximum dimension. This method produced a very good fit for $D < 200\,\mu$m, but it was also applied to larger particles.

Noh et al. [32] found that H04 values were typically 60–80% smaller than the Locatelli and Hobbs [33] values. The estimates from Mitchell [18] have discrepancies in a factor of 2 [21]. Since no direct IWC measurements were available during our field observations, we could not conclude which method had the smallest errors. Considering that the H04 method was based on the measured IWCs, we chose the estimation with the H04 relationship.

2.3. LWC Calculation. The forward scattering spectrometer probe (FSSP) can detect small particle size distributions from the amount of forward scattered light. In comparison, the CAS determines particle sizes from both forward and backward scattered light. And the CDP detects scattered light in all directions when particles pass through the laser beam. For mixed-phase conditions, droplet spectra measured from the FSSP were inevitably contaminated by ice particles and shattering. Cober et al. [34] found that the FSSP measured droplet spectra could be significantly biased by ice crystals for the size range above 35 μm. Further evaluation by Cober et al. [35] demonstrated that the derived LWC agreed with the measured LWC from other probes and within the errors expected from such comparisons. The FSSP measurements of concentration and LWC were found to agree to within ±34% and ±38%, respectively. Therefore, LWC estimated from the FSSP was still used in previous studies [21, 24].

Compared with the FSSP, the improved measurement techniques used in the CAS minimized observation uncertainties [36], although shattering of ice crystals still occurred on the CAS inlet [37]. In comparison, the CDP had no inlet and, differed from the optical mask of the FSSP annulus detector, generally produced less degree of particle shattering and overcounting than the FSSP [38]. The estimated bias for LWC from the CDP was concentration dependent and it could be as low as −80% [39]. It should also be noted that both CAS and CDP have difficulty in distinguishing small ice particles from droplets during observations. However, contamination of small ice particles was not significant in mixed-phase clouds, as most ice particles grew rapidly to

Table 1: Horizontal flight leg features, including aircraft, beginning and end times, altitudes, and cloud temperatures.

No	Date (YYMMDD)	Aircraft	Times (CST-hhmm)	Altitude (km)	Temperature (°C)
Leg 1	100420	Shanxi	1030–1050	3.6	−4.2–−0.4
Leg 2	100420	Beijing	1645–1710	4.3	−4.1–−2.5
Leg 3	100420	Shanxi	1645–1710	3.7	−1.8–−0.4
Leg 4	100421	Shanxi	1035–1055	3.9	−5.1–−4.2
Leg 5	090501	Beijing	0930–1003	3.6	−3.9–−0.5
Leg 6	090501	Shanxi	0930–1015	4.2	−8.5–−5.0
Leg 7	090501	Beijing	1044–1052	4.9	−10.3–−9.7
Leg 8	090418	Shanxi	1730–1810	4.2	−2.2–−1.4

CST: China Standard Time.

larger than 25 μm in less than one minute [40]. Based on above research, it was considered reasonable to estimate LWC from the CAS and CDP probes.

3. Flight Paths

Eight horizontal flight traverses and two ascents within the cold layer associated with three precipitating clouds over northern China were selected in the study. All three cloud cases were multilayered clouds that consisted of primarily altostratus and stratocumulus. The corresponding horizontal flight information is listed in Table 1.

In total, four horizontal flight legs were conducted during 20 and 21 April 2010, including two flight legs in the morning and two other legs in the afternoon. It is worth noting that both legs 2 and 3 were conducted during 1645 and 1710 CST for the same cloud case, except that they were at different horizontal levels. The target region of another three flight legs in 2009 was about 350 km northeast of the observation region in 2010. Similarly, legs 5 and 6 were for the same cloud case except at different horizontal levels. After leg 5, the Beijing aircraft ascended to higher levels and conducted one shorter horizontal observation at 4.9 km. For the cloud case on 18 April 2009, the clouds were in the initialization stage, so no rain was on the surface yet by the time of aircraft observation. The two ascents with the first one from 3.7 to 5.8 km (−1 to −11°C) and the other one from 3.7 to 6.2 km (−1 to −12°C) for the 100420 cloud case were also used to complement horizontal measurements.

4. Horizontal Variation of IWC, LWC, and Particle Habits

The variation of IWC, LWC, and particles habits for the 100420 cloud case was examined in this section. The stratiform clouds on 20 April 2010 were associated with an upper-level trough and surface low-pressure center that moved from southwestern to eastern China. Light-to-moderate rain continued throughout 20 April 2010 and stopped by the early afternoon of the next day over Shanxi Province. Additional radar data in the higher ice region would be more helpful, but they were not available. Therefore, cloud development was shown by observations from a C-band doppler radar with the maximum range of 150 km at Taiyuan (longitude: 112.6°; latitude: 37.7°; ASL: 817.0 m).

Figure 1 shows three plan position indicator (PPI) images and one range height indicator (RHI) image observed by the radar at four selected times (China Standard Time, CST = UTC + 8). Figure 1(a) shows that, at 1031 CST 20 April, rather weak and scattered echo regions around Taiyuan were observed, with one relatively larger region to the southwest of Taiyuan. During 1000 and 1200 CST, light rain with 2 h accumulated rainfall of less than 0.5 mm was observed around Taiyuan.

By 1625 UTC 20 April (Figure 1(b)), the clouds had been more organized with the general reflectivity of 20–30 dBZ and the maximum values increasing to 35–41 dBZ. The 2 h accumulated precipitation during 1600 and 1800 CST increased to 1–6 mm. By 1036 CST 21 April (Figure 1(c)), the clouds had been in the dissipating stage, showing two small separated reflectivity regions with the maximum values of only 15–20 dBZ. The RHI image at 1704 CST 20 April (Figure 1(d)) suggests the typical radar bright band with values of about 30 dBZ at approximately 1.6 km above ground level, indicating weak updrafts inside clouds. The above radar information demonstrated that the 100420 case fell in the range of stratiform cloud precipitation.

Figure 2 shows the time series of IWC and LWC determined by the combined CIP and PIP across the horizontal flight leg 1 on 20 April 2010. The data have been averaged over 10 s to reduce spurious variability. From Figure 2, it can be seen that IWC fluctuated from the peak values of over 0.35 g m^{-3} to relatively lower values of less than 0.05 g m^{-3}, suggesting spatial inhomogeneity of cloud development. In comparison, LWC also varied inside the cloud, including the maximum value of 0.23 g m^{-3} at about 1031 CST and extremely low values of less than 0.01 g m^{-3} at other times. High IWC did not always correspond to high LWC, as many other factors, such relative humidity, cloud temperature, and cloud dynamics, also had impacts on ice particle growth modes. For comparison, two short time periods, one characterized by both high IWC and LWC during 1031 and 1035 CST and the other with both lower IWC and LWC (<0.01 g m^{-3}) during 1044 and 1046 CST, were chosen. The particle images observed during these two periods are shown in Figure 3.

For the first period (Figure 3(a)), there were needles, columns, and unidentifiable crystals in small sizes. It is notable that dendrites and aggregates of dendrites were dominant in this region, with sizes of many aggregates even larger

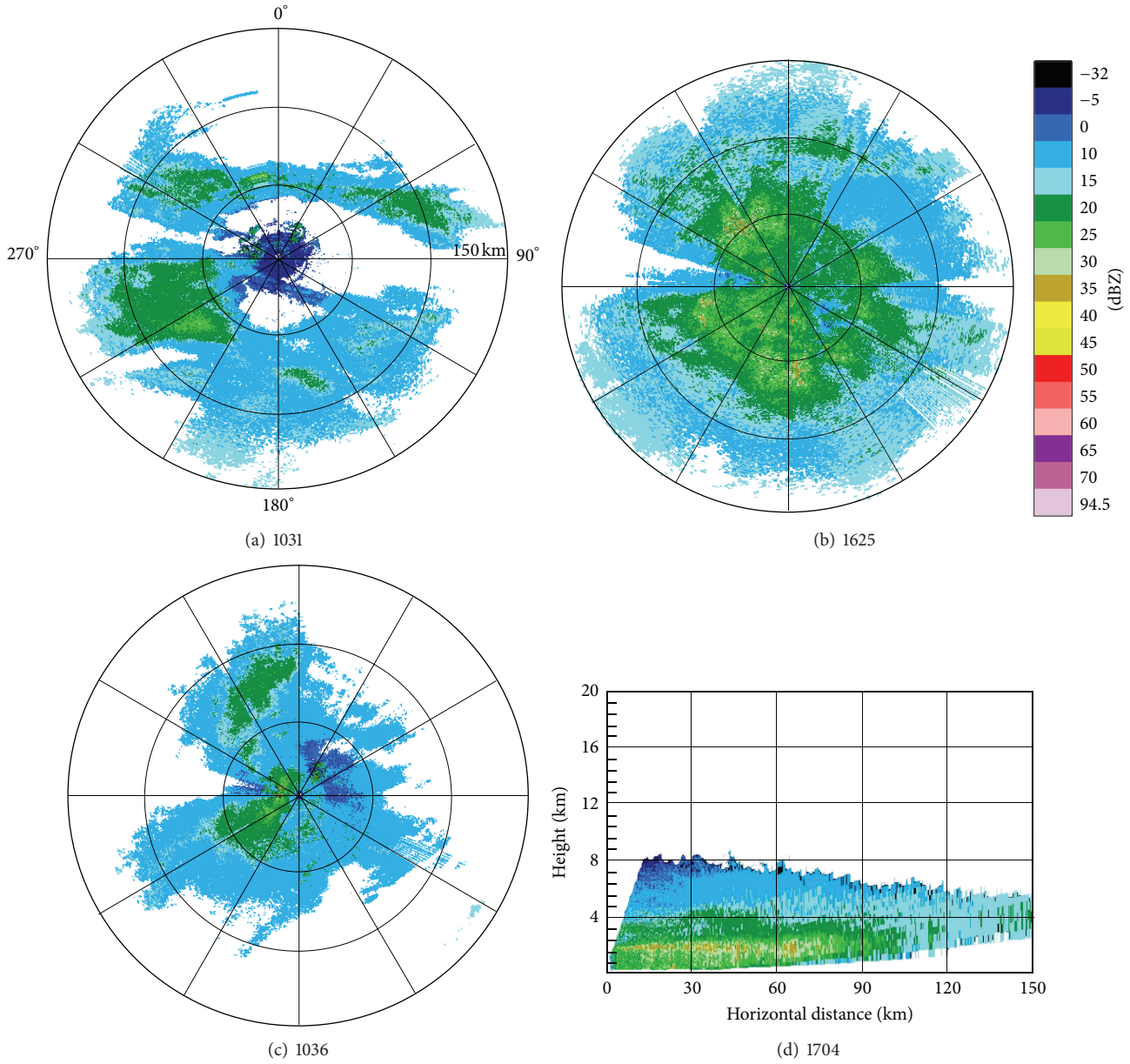

Figure 1: PPI and RHI radar display of the radar reflectivity factor (in dBZ) from the Taiyuan radar at (a) 1031 CST 20 April, (b) 1625 CST 20 April, and (c) 1036 CST 21 April 2010 with an elevation of 1.5° and at (d) 1704 CST 20 April 2010 with the azimuth of 242°. The range markers are 50 and 30 km for PPI and RHI images, respectively.

than the maximum range of the CIP. Well-distinguished branches of dendrites and their assemblages from the PIP suggested that aggregation was the dominant growth mode in that region (about −2 to −1°C). According to past laboratory studies, dendrites should occur most frequently at −15 to −10°C. However, a significant number of dendritic particles were observed at −10 to 0°C level [41], indicating falling of ice particles from the above layer. Therefore, the large dendrites in the study were assumed to fall from colder temperature levels at around or above the 6 km altitude.

For the other region observed during 1044 and 1046 CST (Figure 3(b)), particles sizes were much smaller, with needles, columns, and irregular rimed crystals observed. As the two time periods were both in the environmental temperature of about −2 to −1°C, higher supersaturation with respect to ice aloft during 1031 and 1035 CST was considered as the main factor leading to the fast growth of large dendrites.

The estimated IWC and LWC during the horizontal legs 2 and 3 are shown in Figure 4. IWC values at 4.3 km (around −3.5°C, Figure 4(a)) were significantly high, generally in the range of 1.0–3.0 g m^{-3} and the maximum value of 3.1 g m^{-3}. LWC values at that height were only 0.02–0.06 g m^{-3}. IWC values at lower 3.7 km level (Figure 4(b)) also exhibited high values of 1.1–4.2 g m^{-3}. Overall, LWC values at this level were

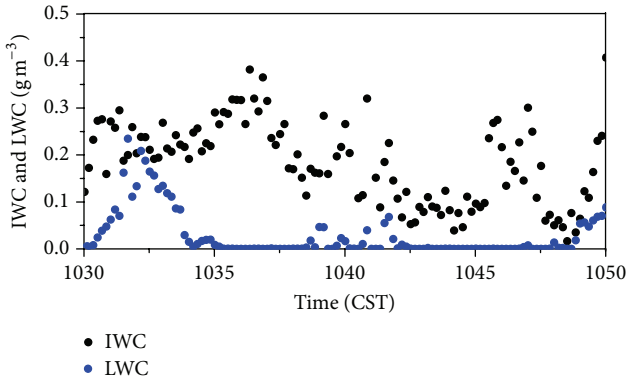

Figure 2: Time series of IWC (black) and LWC (blue) across flight leg 1.

much lower, with some extremely low values of even less than 0.01 g m^{-3}.

Figure 5 shows the ice particle images at selected times during legs 2 and 3. It can be seen in Figure 5(a) that ice particles were predominantly needles, small hollow columns, and combination of needles at 4.3 km at around 1653 CST. Few rimed crystals were also present. For the other region observed during 1700–1710 CST, significant riming was observed, including such rimed particles as branched crystals, radiating assemblage of plates, capped columns, and irregulars. For the 3.7 km level (Figure 5(b)), predominant needles were also present at 165209 CST, while combination of capped columns and branched crystals with obvious riming existed at the other region. On the whole, a significant number of large heavily rimed ice crystals were observed at both 4.3 and 3.7 km. The capped columns were assumed to form as columns at higher levels (−25–−20°C) fell through the planar-crystal region (−18–−12°C), suggesting that the initial columns appeared at least at 7.5 km altitude. In addition, the crystal number concentrations at 4.3 and 3.7 km were over 50 and 100 L^{-1}, respectively, which were much higher than the values calculated from the ice nucleation formula. Therefore, ice seeding from above the cloud layer contributed to the formation of high IWCs.

As shown in Figures 3 and 5, needles dominated along parts of the flight tracks at temperatures > −5°C. This was in agreement with previous observations [41] which found that needles occurred most frequently at temperatures between 0 and −5°C. Therefore, the many detected needles from legs 1 to 3 formed initially at that temperature range and later grow primarily through diffusional growth mechanism.

On the whole, the cloud case was characterized by high IWC values at temperatures above −5°C, with magnitudes from 0.1 to 5 g m^{-3}. In contrast, LWC values were generally rather low with peak values of less than 0.3 g m^{-3} and a small magnitude of 0.01 g m^{-3}. The existence of large dendritic crystals, capped columns, and branched crystals with some degree of riming indicated that ice seeding from the above cloud layer (6 km altitude or above) contributed significantly to both high ice crystal number concentrations and IWCs.

5. Vertical Distribution of IWC with Temperature

IWCs in cirrus generally decreased with decreasing temperature; however, they were considerably scattered, dependent on relative humidity, temperature, vertical velocity, and other particle characteristics [42, 43]. The IWC in single layered mixed-phase clouds maximized in the mid or lower parts of clouds, while higher IWC values might occur in the top of each cloud layer for multilayered clouds [21]. To show the variation of IWC with temperature, Figure 6 presents the IWCs and ice particle concentrations from all the eight horizontal legs listed in Table 1.

According to Figure 6(a), the observations from legs 2 and 3 of the 100420 cloud case suggested general decrease of IWC with decrease of temperature from −1 to −4°C. For the 090501 cloud case, maximum IWC values also decreased from about 2.0 g m^{-3} at −3°C to the magnitude of 0.1 g m^{-3} at −8°C. Comparison of IWCs from legs 5, 6, and 7 suggested that although IWC had decreased to less than 0.1 g m^{-3} at −8°C, higher values of between 0.2 and 0.8 g m^{-3} at even lower −10°C still could be observed, since the two levels belonged to different cloud layers. In addition, predominant low IWC values of less than 0.25 g m^{-3} were also observed at various levels due to different phase of cloud dynamics.

Ice particle concentrations (Figure 6(b)) varied from the small magnitude of 1 L^{-1} to the significant large values of up to 10^2 L^{-1} throughout the layers below −11°C. There was great variability even along the same horizontal flight leg. Ice particle concentrations of up to 10^2 L^{-1} were also observed in stratiform clouds over Northern China due to the existence of embedded convective cells and such process as ice multiplication [26]. Hobbs and Rangno [44] found the high ice particle concentrations of 40 L^{-1} within one stratocumulus layer as there was embedded convection within the cloud.

Therefore, IWC values varied significantly at the same temperature level due to different cloud development stages. The general decrease of IWC with increase of height could be seen within one cloud layer at one certain stage but not throughout the cold layer of multilayered clouds.

In addition to above horizontal flights, two vertical profiles were also obtained for the 100420 cloud case, including one ascent from 3.7 to 5.8 km during 1057 and 1122 CST and the other ascent from 3.7 to 6.2 km during 1723 and 1750 CST. The profiles of IWC, ice particle concentrations from the CIP, and cloud droplet concentrations from the CDP are shown in Figure 7. All the values were averaged over 100 m in the vertical. From Figure 7(a), it can be seen that IWC values in the morning were mostly between 0.1 and 0.6 g m^{-3}, corresponding to the general ice particle concentrations of 10–40 L^{-1} (as shown in Figure 7(b)). The peak IWC value at −8°C corresponded to the high ice particle concentrations of up to 64 L^{-1}. By the afternoon, IWC values at all levels generally had increased significantly to over 0.8 g m^{-3} at most levels. During that stage, ice particle concentrations also increased to over 30 L^{-1} or even up to 151 L^{-1} at −5.5°C.

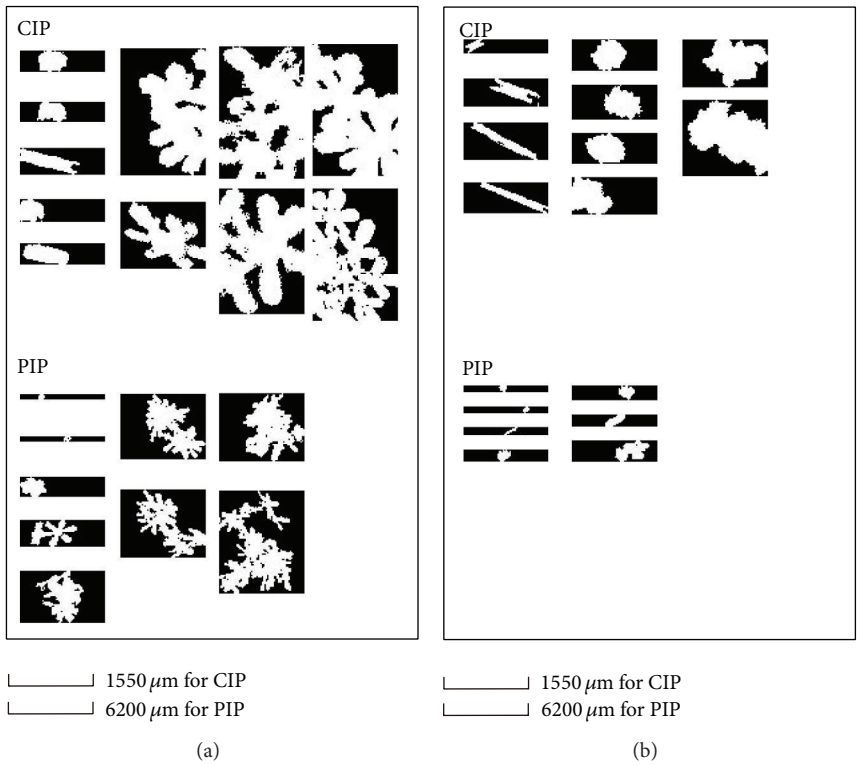

Figure 3: CIP and PIP images across flight leg 1 during (a) 1031–1035 CST and (b) 1044–1046 CST.

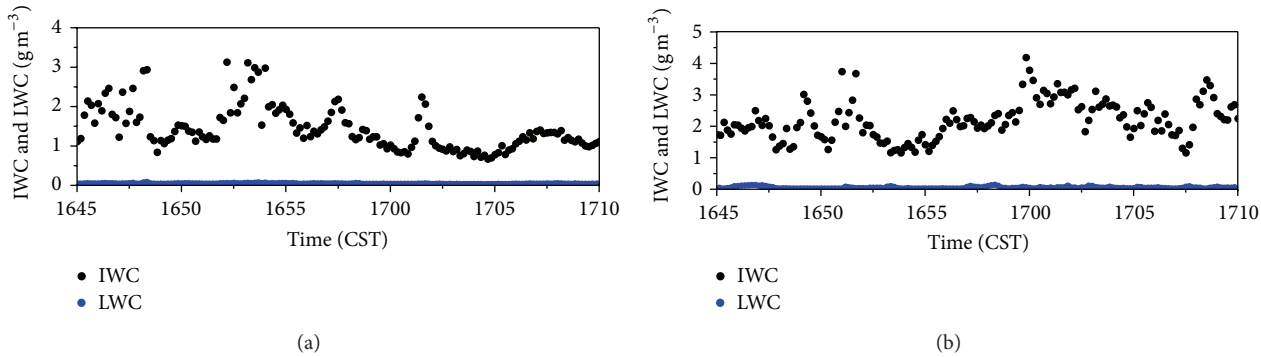

Figure 4: Time series of IWC (black) and LWC (blue) across flight legs (a) 2 and (b) 3.

The overall IWC profiles at these two stages suggested little correlation between IWC and temperature, so IWC does not always decrease with decreasing temperature and was linked more to cloud dynamics which produced different ice particle concentrations. Cloud droplet concentrations at both stages had the extremely low values, with the magnitude of 0.1 cm^{-3} except one peak value of 27 cm^{-3} at −9.1°C.

To show the ice particle characteristics more clearly, Figure 8 presents the 2D images from the CIP during those two vertical ascents. It should be noted that apart from the large particles shown in Figure 8, large numbers of small irregulars also existed in both stages. During the first ascent (Figure 8(a)), large particles were primarily hexagonal plates between the −9 and −11°C level and rimed dendrites below the −9°C level. By the time of the second ascent (Figure 8(b)), particles not only become larger in size, but also changed a lot in habits. Many heavily rimed capped columns, graupel-like snow, and plates appeared at various levels. In addition, aggregates of capped columns and plates also occurred. Based on particle fall-speed measurements by Locatelli and Hobbs [33], densely rimed dendrites, 500–1000 μm in diameter, are assumed to have fall velocities of 2.2 to 2.8 m s^{-1}. In comparison, graupel-like snow of lump type with the same diameter should have fall velocities of between 3.3 to 4.0 m s^{-1} and densely rimed columns have much higher velocity of around 10 m s^{-1}. The updrafts in stratiform clouds are generally in the magnitude of 0.1 m s^{-1}. Therefore, the capped columns and graupel-like snow in the second ascent

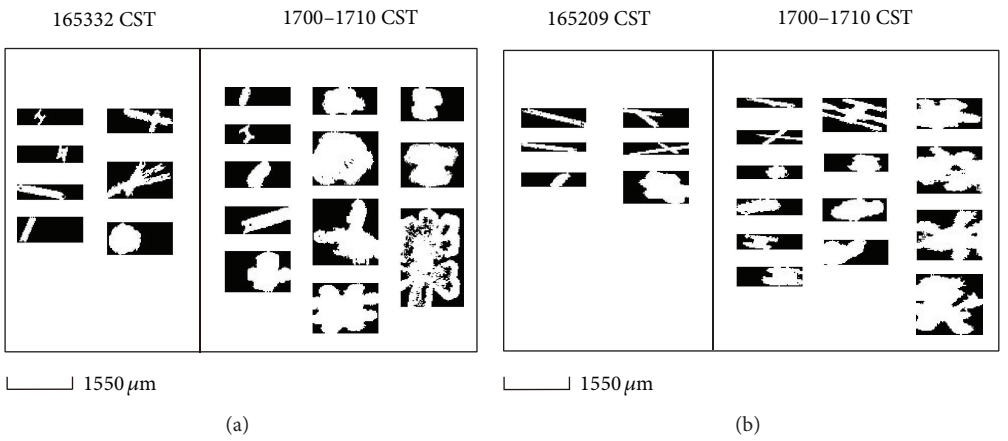

FIGURE 5: CIP images across flight legs (a) 2 and (b) 3 during selected periods.

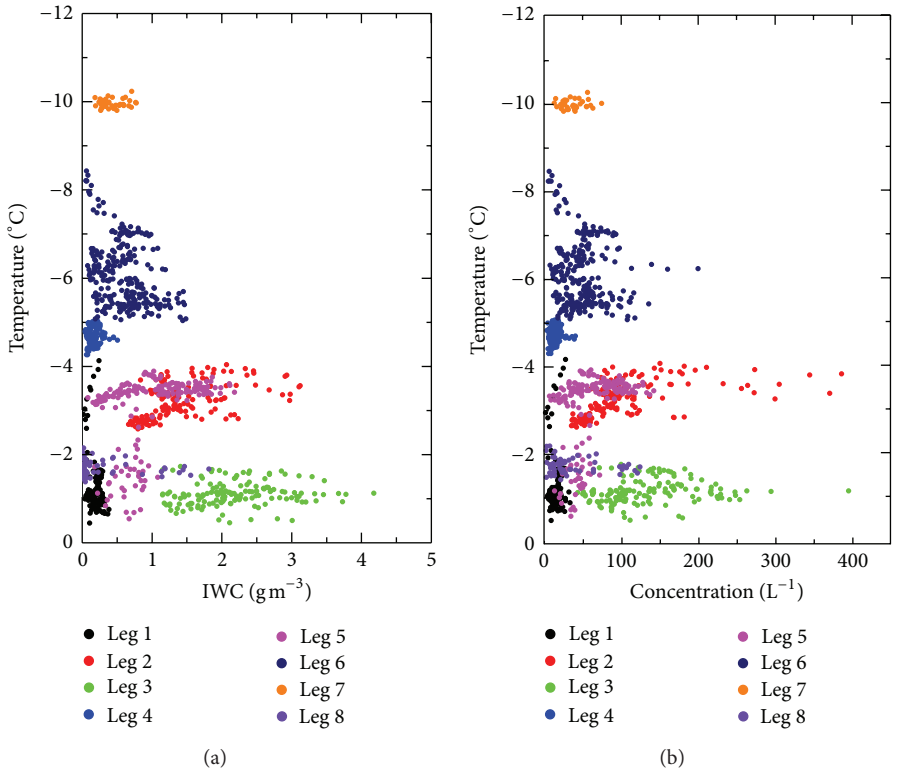

FIGURE 6: Variation of (a) IWC and (b) ice particle concentrations with temperature for the three cloud cases.

were considered to have higher net velocities than those in the first ascent, which contributed to higher IWCs at various temperature levels.

6. Particle Size Distribution and Spectrum Parameters

Ice particle size distributions within clouds over northern China have been fitted in previous studies following an exponential form [14]. However, the data were obtained in the 1980s using OAP-2D-C and OAP-2D-P. The use of new instrumentation in our aircraft measurements is better in providing particle size information. Both exponential and gamma functions were used in the study to parameterize ice particle size distributions. The equation that describes the gamma distribution is

$$N(D) = N_{0\Gamma} D^{\mu} e^{-\lambda_{\Gamma} D}, \quad (2)$$

where $N_{0\Gamma}$, μ, and λ_{Γ} are intercept, dispersion, and slope parameters to be derived. When $\mu = 0$, the gamma fit becomes an exponential function:

$$N(D) = N_0 e^{-\lambda D}. \quad (3)$$

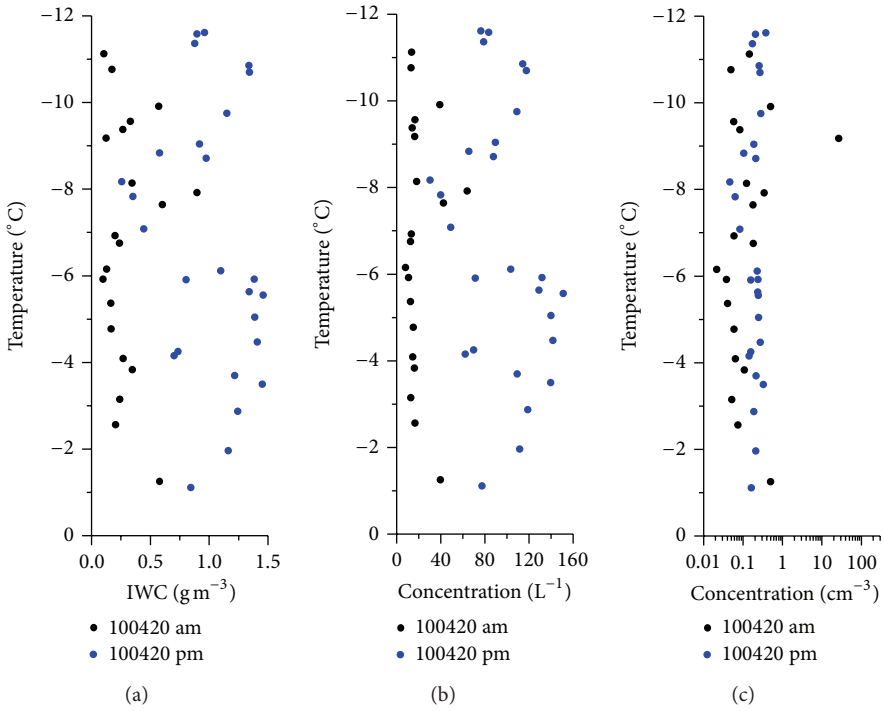

Figure 7: Vertical profiles of (a) IWC (g m^{-3}), (b) ice particle concentrations (L^{-1}) from the CIP and (c) cloud droplet concentrations (cm^{-3}) from the CDP for the 100420 cloud case during the two ascents.

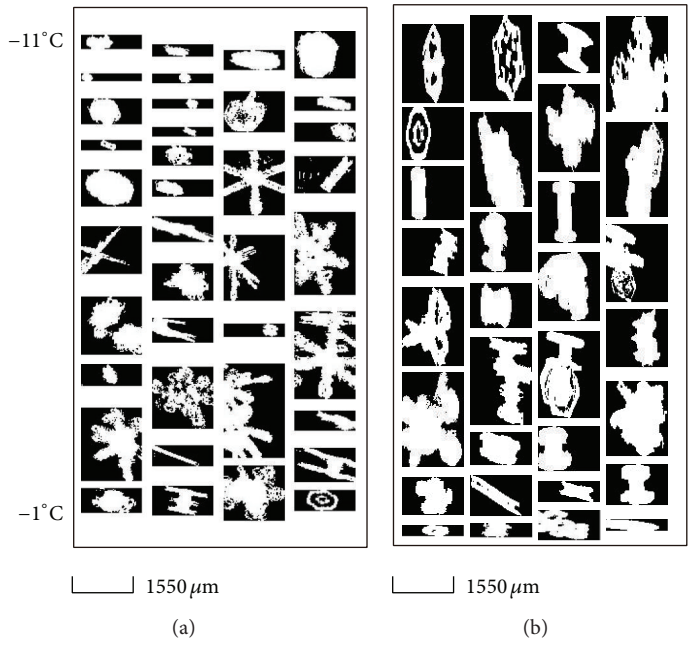

Figure 8: CIP images across the two flight ascents during (a) 1057 and 1122 CST and (b) 1723 and 1750 CST.

As particle size distributions are highly variable from one cloud region to another, Figure 9 firstly shows the average particle size distributions for different legs. Size distributions in Figure 9(a) included particles below 1000 μm detected by the CIP and above 1000 to 6200 μm detected by the PIP. It can be seen that measurements from the two probes overlapped quite well at 1000 μm and most particles were smaller than 2000 μm. For particles larger than 500 to 1000 μm, the concentration (plotted on logarithmic axes) decreased linearly with size (plotted on linear axes), suggesting that above these sizes the particle size distributions were of exponential shape. In contrast, for particles smaller than 500 to 1000 μm, a linear

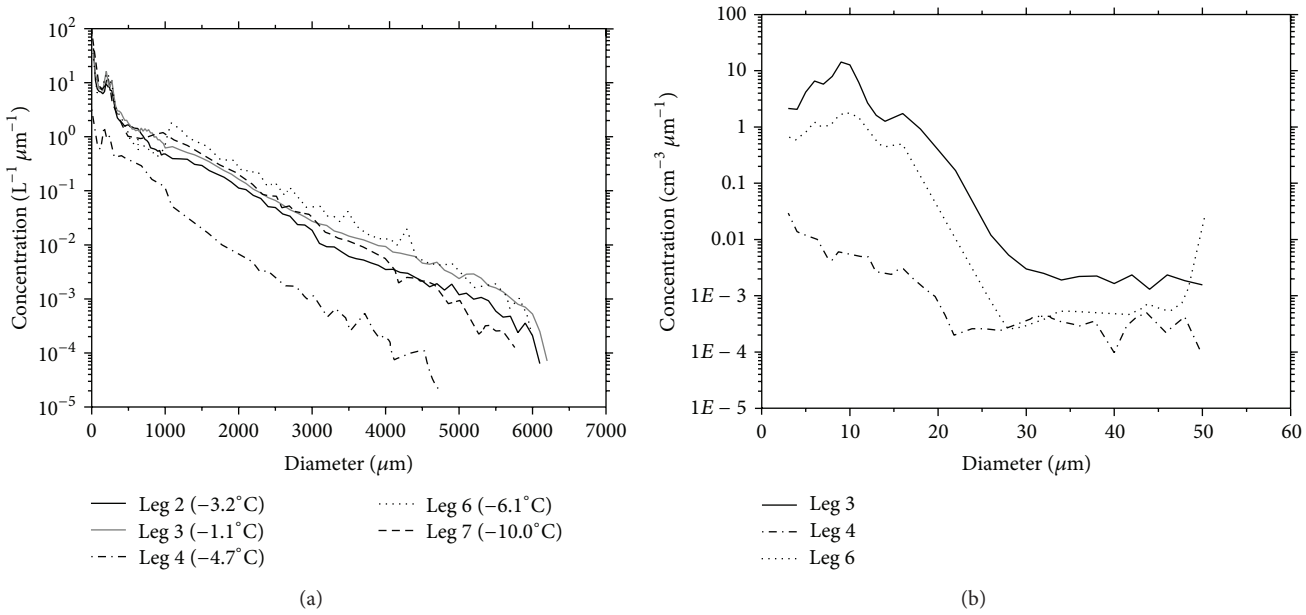

Figure 9: Average particle size distributions for various legs from (a) combined CIP and PIP and (b) CDP.

decrease is not so obvious when plotted on the logarithmic axes. Average particle concentrations measured by the CDP during legs 3, 4, and 6 are plotted in Figure 9(b), which varied significantly for different flight legs. The CDP data were not combined with the CIP measurement for two reasons. On the one hand, the Beijing aircraft was equipped with the CAS, not the CDP. On the other hand, particles in the size range 25–100 μm from the CIP detection were not used in the study, so there was no overlap between 50 (the maximum size bin for the CDP) and 100 μm.

Figure 10 shows the N_0 versus λ and $N_{0\Gamma}$ versus λ_Γ points for the various horizontal legs. Each data point corresponded to a CIP and PIP combined size distribution averaged over 10 s. For the exponential fit (Figure 10(a)), values of N_0 generally had the magnitude of 10^7 to 10^9 m^{-4} and λ values spanned over one order of magnitude. The data were clustered into two groups, including legs 2, 3, 5, 6, and 7 with higher N_0 and lower λ values, as well as legs 1, 4, and 8 with lower N_0 and relatively higher λ values. The λ variation indicated that ice particles during legs 2, 3, 5, 6, and 7 were larger and more concentrated in size, which was in agreement with the occurrence of many rimed and aggregated particles. In comparison, the λ_Γ values (Figure 10(b)) also centered around 10^3 m^{-1} but spanned to over two orders of magnitude.

Plots of μ versus λ_Γ for various legs are shown in Figure 11. The values of μ were between −3 and 4, including evident fluctuations. A relationship similar to that of Heymsfield [4] between μ and λ_Γ was fitted, with the μ values varying from positive values at large λ_Γ to negative values at small λ_Γ. However, due to significant variability in particle size distributions, it was difficult to find an accurate relationship between $N_{0\Gamma}$ and λ_Γ. To compare the fits from exponential and gamma functions, Figure 12 presents correlation coefficients (r^2) versus λ. The correlation coefficients were mostly between 0.6 and 0.9 for both exponential and gamma distributions and also included some scattered lower values. The r^2 value averaged over all exponential fits was 0.68. Similarly, the r^2 value for gamma fits was 0.66. Therefore, the two functions had similar degree of accuracy in fitting particle size distributions.

In addition, plots of particle size spectrum parameters versus cloud temperature and IWC were also examined, but no accurate relationship was found. It is speculated that the data only in a small temperature range of 0 to −5°C from three cloud cases is not enough. To better fit particle size distributions and other related properties, more data of higher quality are still needed.

7. Discussion and Conclusions

This study presented the measurements of ice particle properties observed from horizontal flight legs at selected altitudes as well as from ascent legs for three stratiform precipitating cloud cases. The distributions of IWC, particle habits, and particle size spectrum parameters were examined.

IWC distribution was first analyzed by comparing IWC, LWC, and particle habits from horizontal observations for the 100420 cloud case. Spatial inhomogeneity of IWC was very common in stratiform clouds. High IWC values varying with magnitudes from 0.1 to 5 g m^{-3} were detected below the −5°C level, while LWCs were less than 0.3 g m^{-3}. Needles and hollow columns dominated along parts of flight tracks, indicating that the diffusional growth mechanism was important for the production of relatively smaller ice crystals. At the same time, the occurrence of large dendritic aggregates and rimed particles such as capped columns, branched crystals, and graupel-like snow in the other regions suggested ice seeding from the above layer at around 6-7 km. Those large

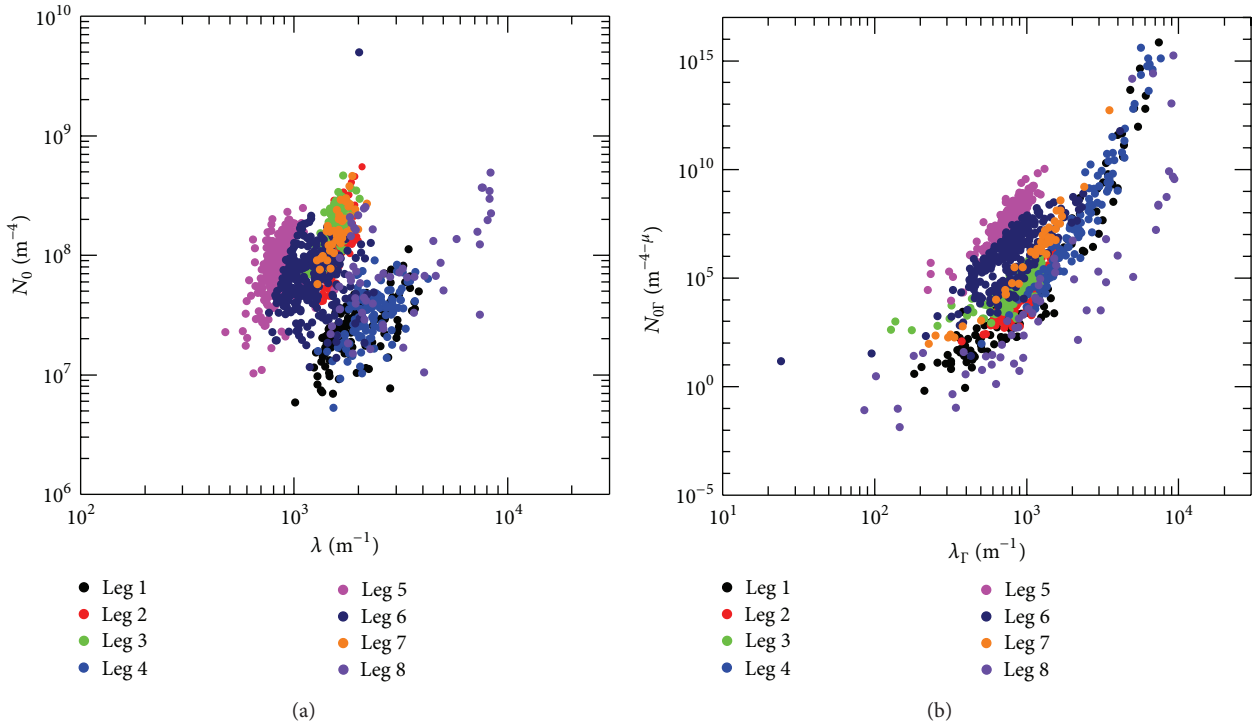

Figure 10: (a) N_0 versus λ and (b) $N_{0\Gamma}$ versus λ_Γ for various legs.

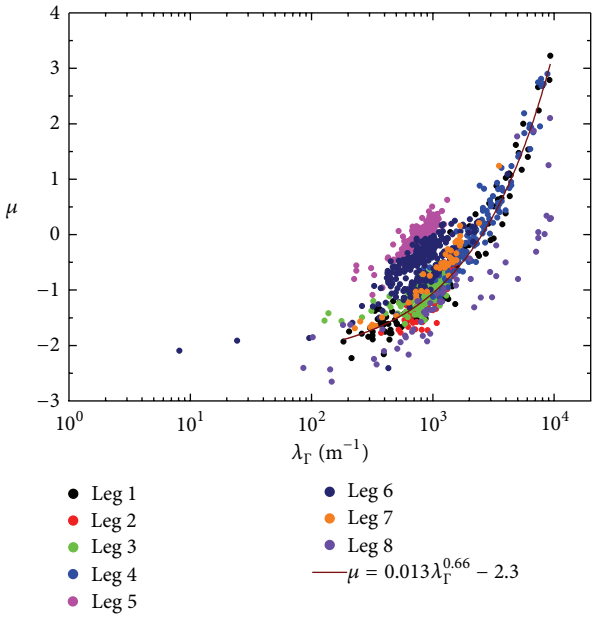

Figure 11: μ versus λ_Γ for various legs.

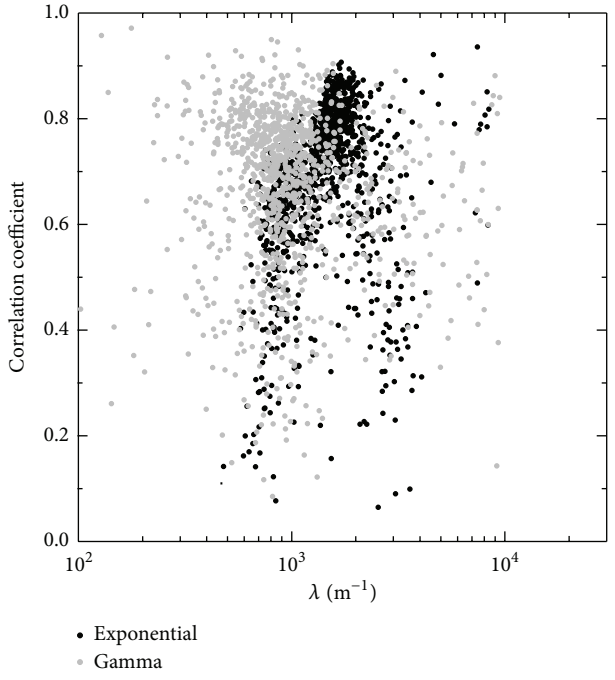

Figure 12: Correlation coefficients for exponential and gamma fits.

rimed particles were also observed during the two ascents, whose relatively higher fall velocities contributed to the appearance of high IWCs at lower levels.

In addition, high IWC also attributed to cloud dynamics. It was speculated that the embedded convection cells contributed to the generation of such high IWC (over 0.5 g m^{-3}), since scattered convective regions with the reflectivity of up to 45 dBZ for the 090501 case and the small reflectivity regions of around 40 dBZ for the 100420 case were observed. By examining layer clouds around the world, Ryan [45] found that deeper stratiform clouds were generally glaciated ones

with embedded convection; however, away from regions of embedded convection the cloud water contents were small.

The stratiform precipitating clouds over northern China are usually multilayered clouds with cirrus, altostratus, and stratocumulus. Vertical variability of IWCs suggested the general decrease trend of IWC maxima with decreasing temperature only in part of the cloud layers, such as the maximum value of more than $4.0\,\mathrm{g\,m^{-3}}$ at $-1^{\circ}\mathrm{C}$ decreasing to around $3.0\,\mathrm{g\,m^{-3}}$ at $-4^{\circ}\mathrm{C}$ in the 100420 case and the maximum $2.1\,\mathrm{g\,m^{-3}}$ at $-3.5^{\circ}\mathrm{C}$ decreasing to less than $0.1\,\mathrm{g\,m^{-3}}$ at $-8.5^{\circ}\mathrm{C}$ in the 090501 case. However, relatively lower IWC values of less than $0.25\,\mathrm{g\,m^{-3}}$ were also observed throughout the cold layer.

On the whole, values of N_0 varied primarily between 10^7 and $10^{10}\,\mathrm{m^{-4}}$ and λ values were generally in the range of 10^3–$10^4\,\mathrm{m^{-1}}$ from exponential distributions. In comparison, both $N_{0\Gamma}$ and λ_Γ spanned more for gamma distributions. Further calculation of correlation coefficients suggested that the two functions had the similar degree of accuracy. By analyzing the slope and intercept parameters for 77 horizontal flight legs, Woods et al. [13] found that values of N_0 varied over three orders of magnitudes and λ values spanned less than a full order of magnitude. Heymsfield et al. [11] found the monotonic relationship between N_0 and λ after using exponential curves to fit particle size distributions for tropical clouds. The small sample size in this study did not allow us to conduct further investigation of the relationship between particle size spectrum parameters and temperature, but the initial analyses were still useful to show the overall characteristics of stratiform clouds over northern China.

Only three cloud cases were examined in this study. To obtain the statistical characteristics of cloud microphysical parameters, a larger sample size is needed. Future work such as analyzing errors in observational data and investigating key parameters affecting aggregation and other microphysical processes should also be conducted.

Conflict of Interests

The authors declare that there is no conflict of interests regarding the publication of this paper.

Acknowledgments

This work was supported by the National Basic Research Program of China (973 Program, Grant no. 2013CB430105), the Strategic Priority Research Program of the Chinese Academy of Sciences (XDA05100300), the National Natural Science Foundation of China (Grant no. 41105095), and the Knowledge Innovation Program of the Chinese Academy of Sciences (Grant no. KZCX2-EW-203).

References

[1] G. M. McFarquhar and A. J. Heymsfield, "Parameterization of tropical cirrus ice crystal size distributions and implications for radiative transfer: results from CEPEX," *Journal of the Atmospheric Sciences*, vol. 54, no. 17, pp. 2187–2200, 1997.

[2] A. V. Korolev, G. A. Isaac, and J. Hallett, "Ice particle habits in Arctic clouds," *Geophysical Research Letters*, vol. 26, no. 9, pp. 1299–1302, 1999.

[3] M. T. Stoelinga, J. D. Locatelli, and C. P. Woods, "The occurence of "irregular" ice particles in stratiform clouds," *Journal of the Atmospheric Sciences*, vol. 64, no. 7, pp. 2740–2750, 2007.

[4] A. J. Heymsfield, "Properties of tropical and midlatitude ice cloud particle ensembles—part II: applications for mesoscale and climate models," *Journal of the Atmospheric Sciences*, vol. 60, no. 21, pp. 2592–2611, 2003.

[5] R. S. Sekhon and R. C. Srivasta, "Snow size spectra and radar reflectivity," *Journal of the Atmospheric Sciences*, vol. 27, no. 2, pp. 299–307, 1970.

[6] R. A. Houze Jr., P. V. Hobbs, P. H. Herzegh, and D. B. Parsons, "Size distributions of precipitation particles in frontal clouds," *Journal of the Atmospheric Sciences*, vol. 36, no. 1, pp. 156–162, 1979.

[7] K. K. Lo and R. E. Passarelli Jr., "The growth of snow in winter storms: an airborne observational study," *Journal of the Atmospheric Sciences*, vol. 39, no. 4, pp. 697–706, 1982.

[8] P. R. Field, "Aircraft observations of ice crystal evolution in an altostratus cloud," *Journal of the Atmospheric Sciences*, vol. 56, no. 12, pp. 1925–1941, 1999.

[9] A. J. Heymsfield, S. Lewis, A. Bansemer et al., "A general approach for deriving the properties of cirrus and stratiform ice cloud particles," *Journal of the Atmospheric Sciences*, vol. 59, no. 1, pp. 3–29, 2002.

[10] G. M. McFarquhar, M. S. Timlin, R. M. Rauber, B. F. Jewett, J. A. Grim, and D. P. Jorgensen, "Vertical variability of cloud hydrometeors in the stratiform region of mesoscale convective systems and bow echoes," *Monthly Weather Review*, vol. 135, no. 10, pp. 3405–3428, 2007.

[11] A. J. Heymsfield, A. Bansemer, P. R. Field et al., "Observations and parameterizations of particle size distributions in deep tropical cirrus and stratiform precipitating clouds: results from in situ observations in TRMM field campaigns," *Journal of the Atmospheric Sciences*, vol. 59, no. 24, pp. 3457–3491, 2002.

[12] P. R. Field, A. J. Heymsfield, and A. Bansemer, "Snow size distribution parameterization for midlatitude and tropical ice clouds," *Journal of the Atmospheric Sciences*, vol. 64, no. 12, pp. 4346–4365, 2007.

[13] C. P. Woods, M. T. Stoelinga, and J. D. Locatelli, "Size spectra of snow particles measured in wintertime precipitation in the pacific northwest," *Journal of the Atmospheric Sciences*, vol. 65, no. 1, pp. 189–205, 2008.

[14] Y. Laiguang and L. Yangang, "Some microphysical characteristics of cloud and precipitation over China," *Atmospheric Research*, vol. 35, no. 2–4, pp. 271–281, 1995.

[15] Z. Deng, C. Zhao, Q. Zhang, M. Huang, and X. Ma, "Statistical analysis of microphysical properties and the parameterization of effective radius of warm clouds in Beijing area," *Atmospheric Research*, vol. 93, no. 4, pp. 888–896, 2009.

[16] J. Ma, X. Guo, C. Zhao, Y. Zhang, and Z. Hu, "Recent progress in cloud physics research in China," *Advances in Atmospheric Sciences*, vol. 24, no. 6, pp. 1121–1137, 2007.

[17] A. G. Hallar, L. M. Avallone, R. L. Herman, B. E. Anderson, and A. J. Heymsfield, "Measurements of ice water content in tropopause region Arctic cirrus during the SAGE III Ozone Loss and Validation Experiment (SOLVE)," *Journal of Geophysical Research D: Atmospheres*, vol. 109, no. 17, Article ID D17203, 2004.

[18] D. L. Mitchell, R. Zhang, and R. L. Pitter, "Mass-dimensional relationships for ice particles and the influence of riming on snowfall rates," *Journal of Applied Meteorology*, vol. 29, no. 2, pp. 153–163, 1990.

[19] P. R. A. Brown and P. N. Francis, "Improved measurements of the ice water content in cirrus using a total-water probe," *Journal of Atmospheric and Oceanic Technology*, vol. 12, no. 2, pp. 410–414, 1995.

[20] A. J. Heymsfield, A. Bansemer, and C. H. Twohy, "Refinements to ice particle mass dimensional and terminal velocity relationships for ice clouds—part I: temperature dependence," *Journal of the Atmospheric Sciences*, vol. 64, no. 4, pp. 1047–1067, 2007.

[21] R. P. Fleishauer, V. E. Larson, and T. H. V. Haar, "Observed microphysical structure of midlevel, mixed-phase clouds," *Journal of the Atmospheric Sciences*, vol. 59, no. 11, pp. 1779–1804, 2002.

[22] M. W. Gallagher, P. J. Connolly, I. Crawford et al., "Observations and modelling of microphysical variability, aggregation and sedimentation in tropical anvil cirrus outflow regions," *Atmospheric Chemistry and Physics*, vol. 12, no. 14, pp. 6609–6628, 2012.

[23] A. J. Heymsfield, C. G. Schmitt, A. Bansemer et al., "Effective ice particle densities for cold anvil cirrus," *Geophysical Research Letters*, vol. 31, no. 2, pp. 1–5, 2004.

[24] L. D. Carey, J. Niu, P. Yang, J. A. Kankiewicz, V. E. Larson, and T. H. V. Haar, "The vertical profile of liquid and ice water content in midlatitude mixed-phase altocumulus clouds," *Journal of the Atmospheric Sciences*, vol. 47, no. 9, pp. 2487–2495, 2008.

[25] Y. Noh, C. J. Seaman, T. H. V. Haar, and G. Liu, "In situ aircraft measurements of the vertical distribution of liquid and ice water content in midlatitude mixed-phase clouds," *Journal of Applied Meteorology and Climatology*, vol. 52, no. 1, pp. 269–279, 2013.

[26] T. Hou, H. Lei, and Z. Hu, "A comparative study of the microstructure and precipitation mechanisms for two stratiform clouds in China," *Atmospheric Research*, vol. 96, no. 2-3, pp. 447–460, 2010.

[27] X. Guo and G. Zheng, "Advances in weather modification from 1997 to 2007 in China," *Advances in Atmospheric Sciences*, vol. 26, no. 2, pp. 240–252, 2009.

[28] A. Korolev and G. A. Isaac, "Shattering during sampling by OAPs and HVPS—part I: snow particles," *Journal of Atmospheric and Oceanic Technology*, vol. 22, no. 5, pp. 528–542, 2005.

[29] A. V. Korolev, E. F. Emery, J. W. Strapp et al., "Small ice particles in tropospheric clouds: fact or artifact? Airborne icing instrumentation evaluation experiment," *Bulletin of the American Meteorological Society*, vol. 92, no. 8, pp. 967–973, 2011.

[30] P. R. Field, A. J. Heymsfield, and A. Bansemer, "Shattering and particle interarrival times measured by optical array probes in ice clouds," *Journal of Atmospheric and Oceanic Technology*, vol. 23, no. 10, pp. 1357–1371, 2006.

[31] D. Bouniol, J. Delanoë, C. Duroure, A. Protat, V. Giraud, and G. Penide, "Microphysical characterisation of West African MCS anvils," *Quarterly Journal of the Royal Meteorological Society*, vol. 136, no. S1, pp. 323–344, 2010.

[32] Y.-J. Noh, C. J. Seaman, T. H. V. Haar, D. R. Hudak, and P. Rodriguez, "Comparisons and analyses of aircraft and satellite observations for wintertime mixed-phase clouds," *Journal of Geophysical Research D: Atmospheres*, vol. 116, no. 18, Article ID D18207, 2011.

[33] J. D. Locatelli and P. V. Hobbs, "Fall speeds and masses of solid precipitation particles," *Journal of Geophysical Research*, vol. 79, no. 15, pp. 2185–2197, 1974.

[34] S. G. Cober, G. A. Isaac, A. V. Korolev, and J. W. Strapp, "Assessing cloud-phase conditions," *Journal of Applied Meteorology*, vol. 40, no. 11, pp. 1967–1983, 2001.

[35] S. G. Cober, G. A. Isaac, and J. W. Strapp, "Characterizations of aircraft icing environments that include supercooled large drops," *Journal of Applied Meteorology*, vol. 40, no. 11, pp. 1984–2002, 2001.

[36] D. Baumgardner, H. Jonsson, W. Dawson, D. O'Connor, and R. Newton, "The cloud, aerosol and precipitation spectrometer: a new instrument for cloud investigations," *Atmospheric Research*, vol. 59-60, pp. 251–264, 2001.

[37] G. M. McFarquhar, J. Um, M. Freer, D. Baumgardner, G. L. Kok, and G. Mace, "Importance of small ice crystals to cirrus properties: observations from the Tropical Warm Pool International Cloud Experiment (TWP-ICE)," *Geophysical Research Letters*, vol. 34, no. 13, Article ID L13803, 2007.

[38] J. Crosier, K. N. Bower, T. W. Choularton et al., "Observations of ice multiplication in a weakly convective cell embedded in supercooled mid-level stratus," *Atmospheric Chemistry and Physics*, vol. 11, no. 1, pp. 257–273, 2011.

[39] S. Lance, C. A. Brock, D. Rogers, and J. A. Gordon, "Water droplet calibration of the Cloud Droplet Probe (CDP) and in-flight performance in liquid, ice and mixed-phase clouds during ARCPAC," *Atmospheric Measurement Techniques*, vol. 3, no. 6, pp. 1683–1706, 2010.

[40] R. P. Lawson, B. A. Baker, C. G. Schmitt, and T. L. Jensen, "An overview of microphysical properties of Arctic clouds observed in May and July 1998 during FIRE ACE," *Journal of Geophysical Research D: Atmospheres*, vol. 106, no. 14, pp. 14989–15014, 2001.

[41] A. Korolev, G. A. Isaac, and J. Hallett, "Ice particle habits in stratiform clouds," *Quarterly Journal of the Royal Meteorological Society*, vol. 126, no. 569, pp. 2873–2902, 2000.

[42] A. J. Heymsfield and L. J. Donner, "A scheme for parameterizing ice-cloud water content in general circulation models," *Journal of the Atmospheric Sciences*, vol. 47, no. 15, pp. 1865–1877, 1990.

[43] A. J. Heymsfield and G. M. McFarquhar, "High albedos of cirrus in the tropical pacific warm pool: microphysical interpretations from CEPEX and from Kwajalein, Marshall Islands," *Journal of the Atmospheric Sciences*, vol. 53, no. 17, pp. 2424–2451, 1996.

[44] P. V. Hobbs and A. L. Rangno, "Ice particle concentrations in clouds," *Journal of the Atmospheric Sciences*, vol. 42, no. 3, pp. 2523–2549, 1985.

[45] B. F. Ryan, "On the global variation of precipitating layer clouds," *Bulletin of the American Meteorological Society*, vol. 77, no. 1, pp. 53–70, 1996.